

1 **Contrasting ocean-atmosphere dynamics mediate flood hazard across the**
2 **Mississippi River basin**

3
4 Samuel E. Muñoz^{a,b}, Brynnydd Hamilton^a, B. Parazin^a

5 *^aDepartment of Marine & Environmental Sciences, Northeastern University, Marine Science Center, Nahant MA,*
6 *USA*

7 *^bDepartment of Civil & Environmental Engineering, Northeastern University, Boston MA, USA*

8
9 *Corresponding author: Samuel E. Muñoz, s.munoz@northeastern.edu*

10
11 **ABSTRACT**

12 The Mississippi River basin drains nearly half of the contiguous United States, and its rivers
13 serve as economic corridors that facilitate trade and transportation. Flooding remains a perennial
14 hazard on the major tributaries of the Mississippi River basin, and reducing the economic and
15 humanitarian consequences of these events depends on improving their seasonal predictability.
16 Here, we use climate reanalysis and river gage data to document the evolution of floods on the
17 Missouri and Ohio Rivers — the two largest tributaries of the Mississippi River — and how they
18 are influenced by major modes of climate variability centered in the Pacific and Atlantic Oceans.
19 We show that the largest floods on these tributaries are preceded by the advection and
20 convergence of moisture from the Gulf of Mexico following distinct atmospheric mechanisms,
21 where Missouri River floods are associated with heavy spring and summer precipitation events
22 delivered by the Great Plains Low-Level Jet, while Ohio River floods are associated with frontal
23 precipitation events in winter when the North Atlantic subtropical high is anomalously strong.
24 Further, we demonstrate that the El Niño-Southern Oscillation can serve as a precursor for floods
25 on these rivers by mediating antecedent soil moisture, with Missouri River floods often preceded
26 by a warm eastern tropical Pacific (El Niño) and Ohio River floods often preceded by a cool
27 eastern tropical Pacific (La Niña) in the months leading up peak discharge. Finally, we use recent
28 floods in 2019 and 2021 to demonstrate how linking flood hazard to sea surface temperature
29 anomalies holds potential to improve seasonal predictability of hydrologic extremes on these
30 rivers.

31 **1. Introduction**

32 The Mississippi River basin is the largest drainage network in North America, and predicting
33 high flows along its rivers is critical for navigation, infrastructure planning, flood mitigation, and
34 emergency response. The Mississippi River and its major tributaries — the Ohio and Missouri
35 Rivers — have long served as economic corridors for the transportation of goods, generation of
36 hydroelectric power, and industrial and agricultural activity (Knox 2007). Flooding represents a
37 perennial hazard that disrupts these activities (Camillo 2012), with the costs of recent flooding in
38 2019, for example, estimated to have exceeded \$20 billion in total economic losses (NCEI 2021).
39 Despite their severe economic consequences, predicting flooding on these rivers remains
40 challenging, with long-range probabilistic outlooks based on current and forecast hydrologic
41 conditions providing a lead time of 1–3 months (Lincoln and Graschel 2016; 2018; NOAA
42 2016). One approach to extend and improve long-range forecasts involves using the connections
43 between hydrologic extremes and coupled modes of ocean-atmosphere variability (Hamlet and
44 Lettenmaier 1999; Wang and Eltahir 1999; Schöngart and Junk 2007) that evolve gradually and
45 control the influx and convergence of moisture to the North American continental interior
46 (Ropelewski and Halpert 1986; Chen and Kumar 2002; Muñoz and Dee 2017).

47

48 Analyses of hydrologic extremes over midcontinental North America emphasize the roles of
49 synoptic scale features and sea surface temperature anomalies in generating both droughts and
50 pluvials (Seager et al. 2005; E.R. Cook et al. 2007; Feng et al. 2011; B.I. Cook et al. 2011; 2014;
51 Coats et al. 2016). Of particular interest for precipitation extremes in this region are the position
52 and strength of the North Atlantic Subtropical High (NASH; Li et al. 2011; Smith and Baeck
53 2015) and the strength of the Great Plains Low Level Jet (GPLLJ; Weaver and Nigam 2008;
54 Dirmeyer and Kinter 2009; 2010; Zhang and Villarini 2019) — both of which regulate the
55 advection of moisture from the Gulf of Mexico towards the Mississippi River basin. Relatedly,
56 both the North Atlantic Oscillation (NAO) and Pacific-North American Pattern (PNA), represent
57 modes of atmospheric variability that mediate meridional moisture transport into the Mississippi
58 River basin (Harding & Snyder 2015; Mallakpour & Villarini 2016; Malloy & Kirtman 2020).
59 Through its influence on the position and strength of the polar and subtropical jets, the El Niño-
60 Southern Oscillation (ENSO) also influences precipitation patterns over the Mississippi River

61 basin, with warm eastern equatorial Pacific sea surface temperatures (El Niño) enhancing winter
62 and spring precipitation over the Great Plains and Gulf Coast and cool eastern equatorial Pacific
63 sea surface temperatures (La Niña) enhancing precipitation over the Ohio River valley
64 (Ropelewski and Halpert 1986). At the same time, sea surface temperature anomalies over the
65 North Atlantic have also been associated with mediating streamflow near the outlet of the
66 Mississippi River basin through its influence on the position and strength of the North Atlantic
67 Subtropical High (Enfield et al., 2001; Muñoz et al., 2018). These features and related
68 atmospheric and oceanic mechanisms have been variously ascribed to historic flood events on
69 the Missouri (Parrett et al. 1993; Kunkel et al., 1994; Arritt et al. 1997; Dirmeyer and Kinter
70 2009; Hoerling et al. 2013), Ohio and lower Mississippi Rivers (Lott and Meyers 1956;
71 Nakamura et al. 2013; Therrell and Bialecki 2015; Smith and Baeck 2015), although the
72 importance and timing of different mechanisms on these tributaries remains unclear. As a result,
73 a unified model describing how hydrologic extremes on the major tributaries of the Mississippi
74 River basin are mediated by ocean-atmosphere variability has yet to emerge.

75

76 Here, we examine the atmospheric and oceanic circulation patterns that generate large floods on
77 the principal tributaries of the Mississippi River basin using a climate reanalysis and river gage
78 data. We focus on all of the largest observed floods (recurrence period ≥ 10 years) for the period
79 1870–2018 on the lower reaches of the Missouri and Ohio Rivers to evaluate the large-scale
80 atmosphere-ocean conditions that contribute to major floods on these rivers. We show that the
81 seasonality and atmospheric mechanisms that trigger floods on these two tributaries differ.
82 Further, we propose that the state of ENSO mediates antecedent moisture over these sub-basins
83 and often serves as a precursor for enhanced flood hazard on the major tributaries of the
84 Mississippi River Basin. Finally, we evaluate recent floods that primarily affected the Missouri-
85 Mississippi Rivers (2019) and Ohio River (2021) to illustrate the contrasting conditions that
86 preceded these floods.

87 **2. Data and methodology**

88 *a. Hydrologic datasets*

89 River discharge and stage data are obtained from the United States Geological Survey (USGS)
90 Water Data for the Nation (USGS 2021). We extracted peak annual discharges from gages with

91 relatively long and continuous records on the lower reaches of the targeted rivers, namely the
92 Missouri River at Hermann (USGS gage number 06934500) and Ohio River at Louisville
93 (03294500) (Figure 1). These gages include historic peaks back to AD 1844 on the Missouri
94 River and AD 1832 on the Ohio River, although here we limit our analyses to events after 1870
95 due to the limited availability and reliability of reanalysis data and gridded observations before
96 this time (Slivinski et al. 2019). We computed the empirical recurrence interval for all annual
97 discharge maxima between 1870–2017 using the equation:

98
$$\text{Recurrence interval} = \frac{(n + 1)}{m}$$

99 where n is the total number of annual maxima in the gage and m is the rank (in descending order)
100 of the event. We then selected all events with recurrence intervals >10 years at each gage, and
101 focused subsequent analyses on these flood events (Table 1). We focus on floods with recurrence
102 intervals ≥ 10 years to isolate the atmospheric and oceanic processes that mediate the largest
103 events on these rivers. These flood events rank among the largest floods by discharge since 1870
104 at other long gage records on the lower reaches of the targeted tributaries, including the Missouri
105 River at St. Joseph (06818000) and Ohio River at Evansville (0332200), and thus are considered
106 representative of large floods on the lower Missouri and Ohio Rivers. To more closely examine
107 the recent 2019 and 2021 floods, we extracted peak stage and discharge data from all gages
108 within the Mississippi River basin for the water year (e.g., October 1 2018 to September 30 2019
109 for the 2019 water year), and classified each gage's peak annual stage based on its stage category
110 (e.g., major flood stage, moderate flood stage).

111

112 *b. Atmospheric and oceanic datasets*

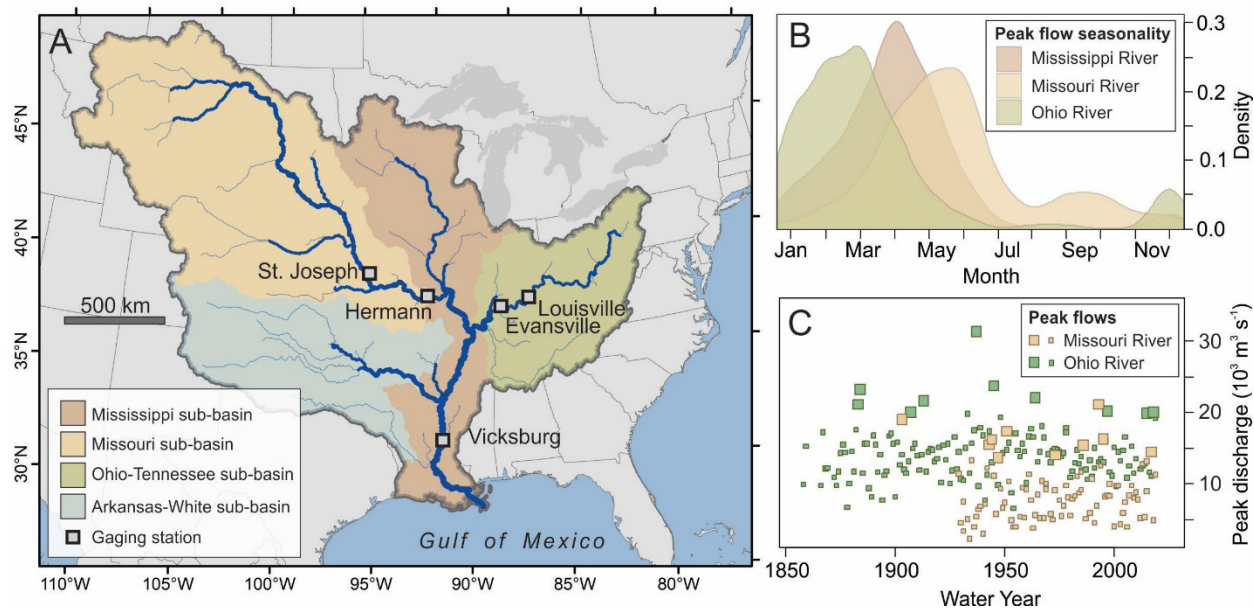
113 To examine the atmospheric patterns associated with the largest observed floods, we examined
114 geopotential height and winds from the National Centers for Environmental Prediction (NCEP)
115 20th century reanalysis version 3 (V3; Slivinski et al., 2019). For each flood event, we extracted
116 daily 850 hPa geopotential heights, u-wind, v-wind, soil moisture, precipitation, and runoff for
117 the 30 days preceding the flood and computed a standard score anomaly based on a long-term
118 mean and standard deviation for the period 1981–2010. We examined aggregate behavior for
119 each tributary by computing the mean of geopotential height, wind, soil moisture, precipitation,
120 and runoff anomalies prior to all events for a given tributary, and expressing these anomalies in

121 terms of standard deviations (σ) from the mean. We computed the significance of these
122 anomalies by bootstrapping with 10,000 random samples of the same length drawn from each
123 variable, and used the resulting distribution to estimate the 10th and 90th percentiles. We also
124 used the meridional wind field from the V3 reanalysis to compute a daily GPLLJ index based on
125 the methodology described in Weaver & Nigam (2008) (i.e., 850 hPa meridional wind anomaly
126 in the core GPLLJ region of 25°–35°N, 102°–97°W), and examined the aggregate (mean)
127 behavior of the GPLLJ in the 60 days before and after flood events. We also obtained a daily
128 NAO index from Cropper et al. (2015) and Hurrell et al. (2003), and examined aggregate
129 behavior of the NAO in the 60 days before and after flood events on each tributary. Finally, we
130 used the Extended Reconstructed Sea Surface Temperature (ERSST v5; Huang et al. 2017) to
131 examine sea surface temperature anomalies associated with flood events, specifically on the
132 Niño3.4 index which we calculated using the methodology described by Trenberth (1997). To
133 compute the significance of these aggregate anomalies, we used bootstrapping where 10,000
134 random samples were drawn from the indices, and estimated the 10th and 90th percentiles of the
135 resulting distributions.

136 **3. A tale of two tributaries**

137 The Missouri and Ohio Rivers — the two major tributaries of the Mississippi River basin —
138 respectively drain the western and eastern portions of the basin, and differ in their physiography
139 and hydroclimatology (Figure 1a). To the west, the Missouri River basin is bounded by the
140 Rocky Mountains and is characterized by the continental and semi-arid climate of the Great
141 Plains (Wise et al. 2018). Within the Missouri River basin, total annual precipitation decreases
142 with distance from the Gulf of Mexico, ranging from ~80 cm near the Missouri River's
143 confluence with the Mississippi River at St. Louis, Missouri to ~40 cm near the Missouri River
144 headwaters near Helena, Montana (Knox 2007). Temperature and precipitation patterns of the
145 Missouri River basin are characterized by strong seasonal contrasts in temperature and
146 precipitation, with 60–80% of total annual precipitation delivered during the warm spring and
147 summer months (March–August) (Muñoz et al. 2020). In contrast, much of the Ohio River basin
148 is characterized by a humid subtropical climate with mild winter temperatures and higher total
149 annual precipitation (100–120 cm) that is distributed more evenly throughout the year (Knox
150 2007). The Ohio River basin is bounded to the east by the Appalachian Mountains, with the Ohio

151 River itself draining into the lower Mississippi River at Cairo, Illinois — roughly 240 km
152 downstream from the confluence of the Missouri and upper Mississippi Rivers.
153



154
155
156 **Figure 1.** The Mississippi River basin and its principal tributaries: (A) major sub-basins of the
157 Mississippi River basin and gaging stations referred to in text; (B) seasonal timing of peak
158 annual discharges of the lower Mississippi River (Vicksburg gage 07289000), Missouri River
159 (Hermann gage), and Ohio River (Louisville gage) expressed as a density function of all water
160 years in the instrumental record; (C) peak annual discharges from the Missouri River at Hermann
161 and Ohio River at Louisville for water years AD 1850–2017, with larger symbols denoting the
162 largest ten events at each gage.
163

164 As a result of their hydroclimatic contrasts, the Ohio and Missouri Rivers differ in the
165 seasonality (Figure 1b) and magnitude (Figure 1c) of their peak flows. Peak annual flows on the
166 lower Ohio River tend to occur in the winter or early spring, with the ten largest historic floods at
167 Louisville, Kentucky cresting between January and April (Table 1). Floods on the Missouri
168 River, in contrast, tend to occur in the spring or summer, with the largest events at Hermann,
169 Missouri cresting between May and October. Streamflow on the Missouri and Ohio Rivers is
170 influenced by infrastructure (Smith and Winkley, 1996; Pinter et al., 2008), particularly by the
171 presence of dams and reservoirs on the upper Missouri River (Wise et al., 2018). An east-to-west
172 precipitation gradient in across the Mississippi River basin ensures that the Ohio River — despite
173 its basin encompassing only ~15% of the total Mississippi River basin — is associated with
174 higher magnitude peak flows than the Missouri River, and is the dominant contributor of

175 discharge to the Mississippi River (Keown et al. 1986). The seasonality of peak annual flows on
176 the lower Mississippi River tends to follow those of the Ohio River, occurring predominantly in
177 spring (March–May). These hydroclimatic contrasts among the major tributaries of the
178 Mississippi River basin are reflected in the different atmospheric and oceanic circulation patterns
179 that precede major flood events on these rivers, which we examine next.

180

181 **Table 1.** Largest floods (recurrence interval ≥ 10 years) by peak daily discharge on the Missouri
182 River at Hermann and Ohio River at Louisville from 1870–2017.

183

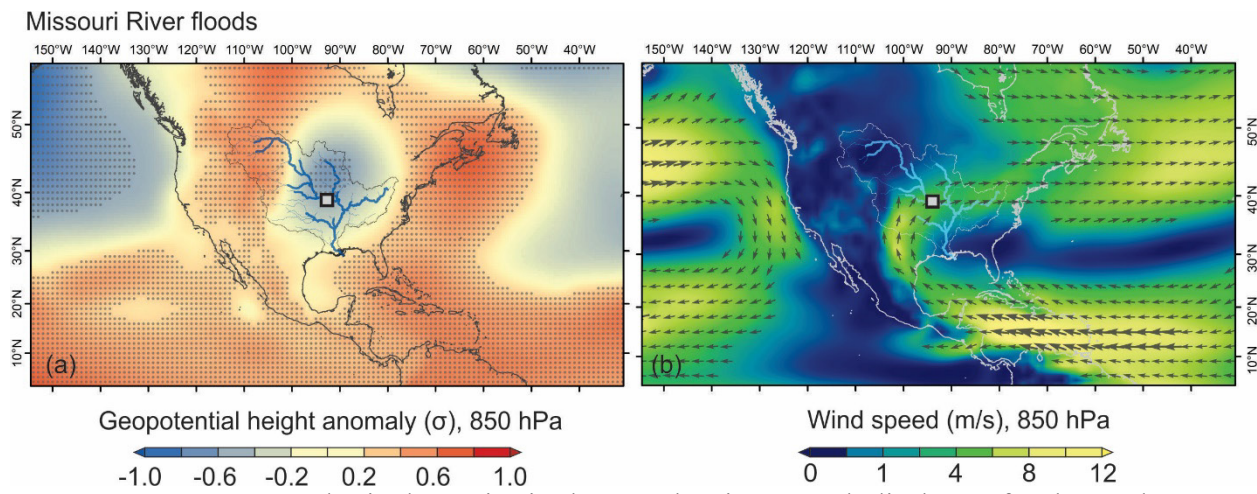
Event No.	Missouri River at Hermann			Ohio River at Louisville		
	Peak date	Peak discharge (m ³ /s)	Recurrence interval (years)	Peak date	Peak discharge (m ³ /s)	Recurrence interval (years)
1	July 31, 1993	21,240	91	January 26, 1937	31,430	148
2	June 7, 1903	19,820	46	March 7, 1945	23,870	74
3	July 19, 1951	19,140	30	February 16, 1884	23,360	50
4	May 19, 1995	17,500	23	March 12, 1964	22,230	37
5	April 28, 1944	16,400	18	April 2, 1913	21,780	30
6	May 21, 1943	16,340	15	February 16, 1883	21,240	25
7	October 5, 1986	15,570	13	March 6, 1997	20,270	21
8	May 4, 2017	15,550	12	January 22, 1907	20,190	19
9	April 25, 1973	14,580	11	March 16, 2015	19,990	16
10	June 29, 1947	14,160	10	March 23, 1933	19,990	15

184 **4. Hydrometeorological mechanisms that generate floods**

185 The atmospheric circulation patterns associated with the largest historical floods on the lower
186 Missouri and Ohio Rivers promote advection and convergence of moisture from the Gulf of
187 Mexico towards the continental interior, but the mechanisms that generate this process differ
188 among the lower Missouri River (Figure 2) and Ohio River (Figure 3). For lower Missouri River

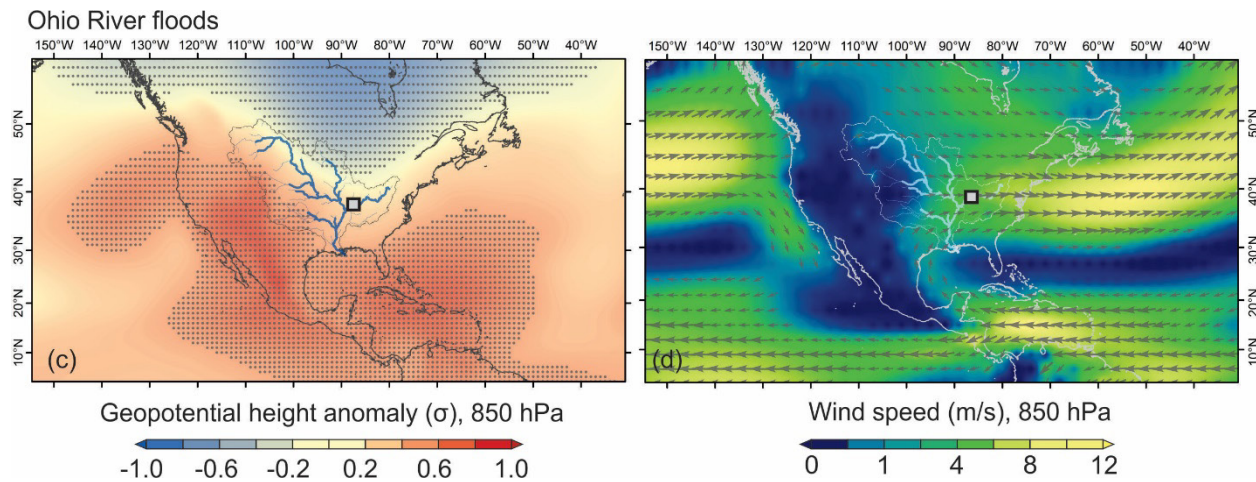
189 floods (Figure 2), aggregate atmospheric behavior in the month of the ten largest historical
 190 floods exhibits a region of anomalously low geopotential height in the lower troposphere (850
 191 hPa level) centered over the Mississippi River basin (Figure 2a). These geopotential height
 192 patterns are accompanied by a directed stream of lower-level winds flowing from the Caribbean
 193 Sea and Gulf of Mexico (Figure 2b) that closely resembles the Great Plains Low Level Jet
 194 (Higgins et al. 1997; Weaver and Nigam 2008) and converges over the Missouri River basin to
 195 produce precipitation over the Missouri River and upper Mississippi River basins (Harding &
 196 Snyder 2015; Malloy & Kirtman 2020). This atmospheric pattern, characterized by a zonally
 197 aligned wave train with significant low geopotential height anomalies over the North Pacific,
 198 Mississippi River basin, and North Atlantic, is similar to the ‘Maya Express’ (Dirmeyer and
 199 Kinter 2009) and ‘Midwest Water Hose’ (Zhang and Villarini 2019) that generate heavy
 200 precipitation events and flooding in the midwestern United States (Weaver & Nigam 2008;
 201 Dirmeyer and Kinter 2010; Malloy & Kirtman 2020). These enhanced low-level jet events occur
 202 in the spring and summer months, represent a major source of warm-season moisture to the
 203 midcontinent (Helfand and Schubert 1995; Mo et al. 1997; Wang and Chen 2009; Algarra et al.
 204 2019), and have been directly linked to lower Missouri River flood events in 1993 and 2008
 205 (Dirmeyer and Kinter 2009). Our analyses link this same mechanism to other large floods of the
 206 lower Missouri River, demonstrating that it precedes the majority of the largest of these floods
 207 (Figure ES1) and is expressed in the aggregate of all large historical floods.

208



210 **Figure 2.** Lower atmospheric dynamics in the month prior to peak discharge for the ten largest
 211 floods on the lower Missouri River (a) geopotential height anomaly (850 hPa) and (b) winds
 212 (850 hPa). Grey boxes denote locations of gage used to define floods. Geopotential height and
 213 wind speeds are expressed as standardized anomalies in terms of standard deviations (σ) from the

214 long-term monthly mean (1981–2010). Stippling in (a) denotes composite anomalies that exceed
215 the 90% confidence interval.
216



217
218
219 **Figure 3.** Lower atmospheric dynamics in the month prior to peak discharge for the ten largest
220 floods on the lower Ohio River (a) geopotential height anomaly (850 hPa) and (b) winds (850
221 hPa). Grey boxes denote locations of gage used to define floods. Geopotential height and wind
222 speeds are expressed as standardized anomalies in terms of standard deviations (σ) from the
223 long-term monthly mean (1981–2010). Stippling in (a) denotes composite anomalies that exceed
224 the 90% confidence interval.
225

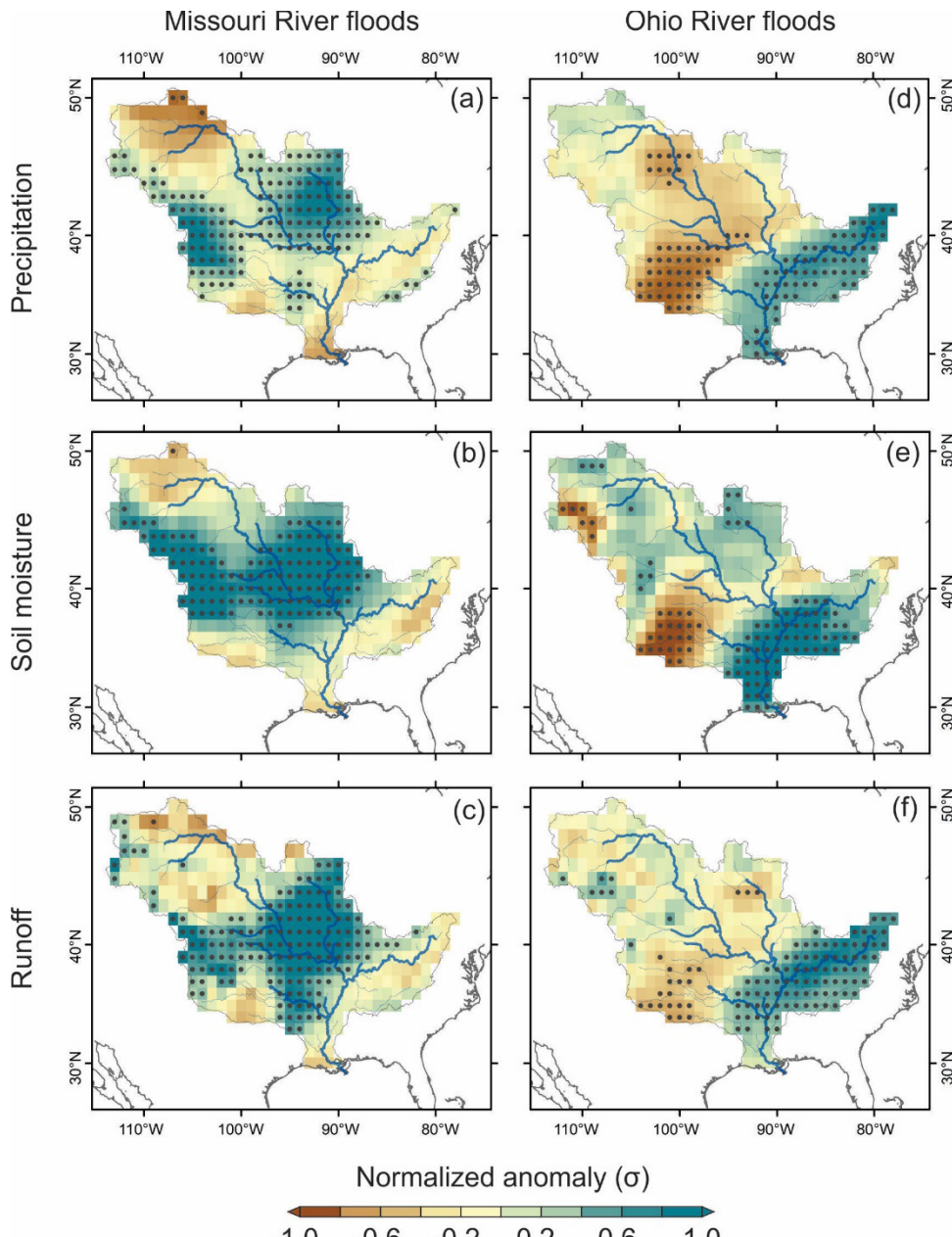
226 In contrast to the large-scale atmospheric patterns associated with floods on the lower Missouri
227 River, aggregate behavior for the ten largest lower Ohio River floods exhibit a low geopotential
228 height anomaly (850 hPa level) over northern North America and high geopotential height
229 anomalies over the North Pacific and North Atlantic that extend into the western United States
230 and Mississippi River basin (Figure 3). These patterns are consistent with strengthened
231 subtropical highs and a positive NAO (Hurrell et al., 2001) which generate lower-level winds
232 that flow from the Caribbean Sea and Gulf of Mexico towards the continental interior and
233 converge over the southeastern United States (Figure 3b) to generate precipitation over the Ohio
234 River and lower Mississippi River basins. An anomalously strong and westerly position of the
235 NASH is present in the month preceding the majority of the largest lower Ohio River floods
236 examined here (Figure ES2), and has previously been attributed to major floods on the lower
237 Mississippi and Ohio Rivers, including the 2011, 1927, and 1937 floods (Lott and Meyers, 1956;
238 Therrell and Bialecki, 2015; Smith and Baeck, 2015). The 1937 event is the flood of record for
239 the lower Ohio River and is integrated into our analyses (Table 1), while the 2011 and 1927
240 events were largely confined to the lower Mississippi River (Camillo, 2012) and were not among

241 the largest events on the lower Ohio River. Our analyses show that this same mechanism —
242 anomalously strong subtropical highs that promote meridional flow off the Gulf of Mexico and
243 convergence over the midcontinent — serves as a trigger for floods on both the lower Ohio and
244 Mississippi Rivers.

245

246 The contrast in the seasonality and atmospheric mechanisms that generate floods between the
247 major western (Missouri River) and eastern (Ohio River) tributaries is also expressed in anomaly
248 fields of key hydrologic variables including precipitation, soil moisture, and runoff (Figure 4). In
249 the month preceding major floods on the lower Missouri River, significant positive anomalies in
250 precipitation, soil moisture, and runoff are situated over the upper Mississippi and Missouri
251 River sub-basins, while the Ohio River basin does not experience anomalously wet conditions
252 during these events (Figure 4a-c). In contrast, significant and positive precipitation, soil
253 moisture, and runoff anomalies shift east to encompass the Ohio River and lower Mississippi
254 River sub-basins in the month preceding major floods on the lower Ohio River (Figure 4d-f).
255 These findings connect the contrasting atmospheric processes associated with floods on the
256 major tributaries of the Mississippi River system to the convergence of atmospheric moisture
257 (precipitation), soil water storage, and runoff.

258



259
260 **Figure 4.** Hydrologic anomalies in the month prior to peak discharge for the ten largest floods on
261 the lower Missouri (left panels) and Ohio Rivers (right panels), including precipitation (top
262 panels), soil moisture (0–40 cm; middle panels), and runoff (lower panels). All fields are
263 expressed as standardized anomalies in terms of standard deviations (σ) from the long-term
264 monthly mean (1981–2010). Stippling denotes composite anomalies that exceed the 90%
265 confidence interval.
266

267

268

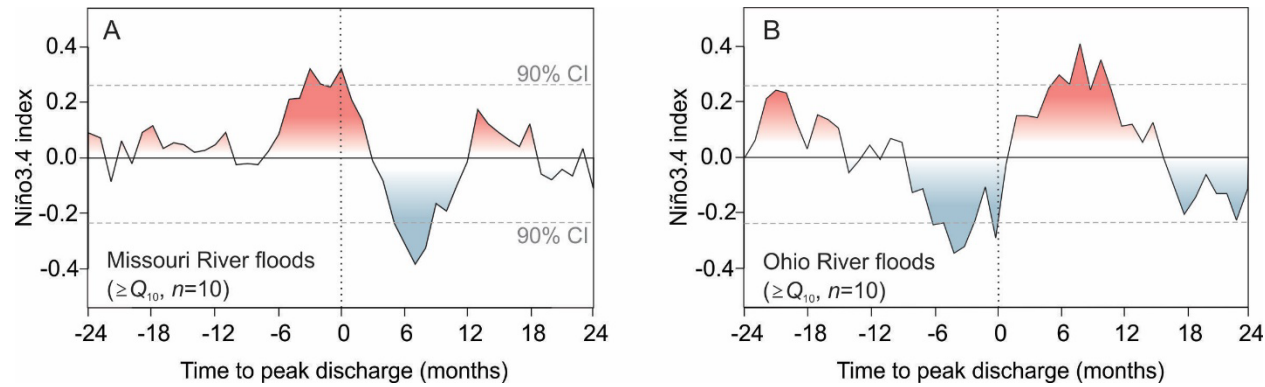
269 Our analyses of geopotential height, wind, precipitation, soil moisture, and runoff fields illustrate
270 the hydrometeorological patterns that directly precede large floods on the major tributaries of the

271 Mississippi River basin: On the lower Missouri River, the month leading up to a flood is
272 characterized by a strengthened GPLLJ and positive moisture anomalies over the Missouri River
273 and upper Mississippi River sub-basins; on the lower Ohio River, the month leading up to a
274 flood is characterized by anomalously strong Pacific and Atlantic subtropical highs and positive
275 moisture anomalies over the Ohio River sub-basin. Both of these mechanisms result in sustained
276 advection of moisture from the Gulf of Mexico that converges over the continental interior in the
277 weeks preceding a flood. These mechanisms represent the dominant atmospheric patterns
278 associated with large floods (> 10 year recurrence interval) on the lower reaches of the tributaries
279 examined here, but we note the variation among individual events (Figures ES1 and ES2) and
280 that other atmospheric patterns can generate large precipitation events in these regions and may
281 be more important for triggering floods on the upper reaches of these tributaries where drainage
282 areas are smaller (Hirschboeck 1988; Smith et al. 2011; Wang and Villarini 2019). While these
283 large-scale atmospheric patterns trigger floods in the weeks prior to an event, we turn next to
284 major modes of climate variability and their influence on flood occurrence to identify precursors
285 that prime the basin in the months leading up to a flood.

286 **5. OCEAN-ATMOSPHERE FORCING OF FLOODS**

287 Over interannual time-scales, flood occurrence on the lower Missouri and Ohio Rivers is related
288 to the evolution of tropical Pacific sea surface temperature anomalies — particularly the El Niño-
289 Southern Oscillation (Figure 5). For lower Missouri River floods, the mean Niño3.4 index of the
290 ten largest floods begins to increase twelve months before peak discharge, exceeding the 90%
291 confidence interval beginning four months prior to the event through to the event itself (Figure
292 5a). The opposite pattern occurs in the months leading up to lower Ohio River floods, where the
293 mean Niño3.4 index of the ten largest floods drops below the 90% confidence interval six
294 months before peak discharge (Figure 5b). These findings imply that, on aggregate, floods on the
295 lower Missouri River are preceded by an anomalously warm eastern equatorial Pacific, while
296 floods on the lower Ohio River are preceded by an anomalously cold eastern equatorial tropical
297 Pacific in the months before peak flow. We note that the evolution of the Niño3.4 index differs
298 among the events evaluated here, with the timing and magnitude of warm or cool sea surface
299 temperature anomalies varying among events (Figure ES3), implying that ENSO represents a
300 mechanism that alters the probability of flood occurrence through its influence on antecedent soil

301 moisture (Muñoz & Dee 2017) but is not a deterministic precursor of flooding. For the ten lower
 302 Missouri River floods considered here, seven (70%) are preceded by El Niño events (defined
 303 here as ≥ 3 consecutive months with $\text{Niño3.4} \geq +0.5$) in the 18 months before the flood (i.e.,
 304 floods in 1993, 1903, 1995, 1943, 1986, 2017, and 1973); a lower proportion (50%) of La Niña
 305 events (defined here as ≥ 3 consecutive months with $\text{Niño3.4} \geq -0.5$) precede lower Ohio River
 306 floods (i.e., floods in 1884, 1964, 1883, 1997, 1907). The evolution of ENSO differs for
 307 individual events, with El Niño/La Niña conditions (i.e., anomalies $+\/- 0.5^\circ\text{C}$) occurring at
 308 different times prior to the event. The long residence time of soil water and groundwater means
 309 that the influence of ENSO on antecedent moisture persists for months after an El Niño/La Niña
 310 event occurs (Chen and Kumar 2002; Lo and Famiglietti 2010; Reager et al. 2014). These
 311 findings — that El Niño and La Niña events often precede large floods on the lower Missouri
 312 and Ohio Rivers, respectively — implicate the El Niño-Southern Oscillation in mediating flood
 313 occurrence on these rivers over interannual time-scales, and extend prior work linking the effect
 314 of El Niño events on antecedent soil moisture and enhanced flood hazard on the lower
 315 Mississippi River (Muñoz and Dee 2017).
 316

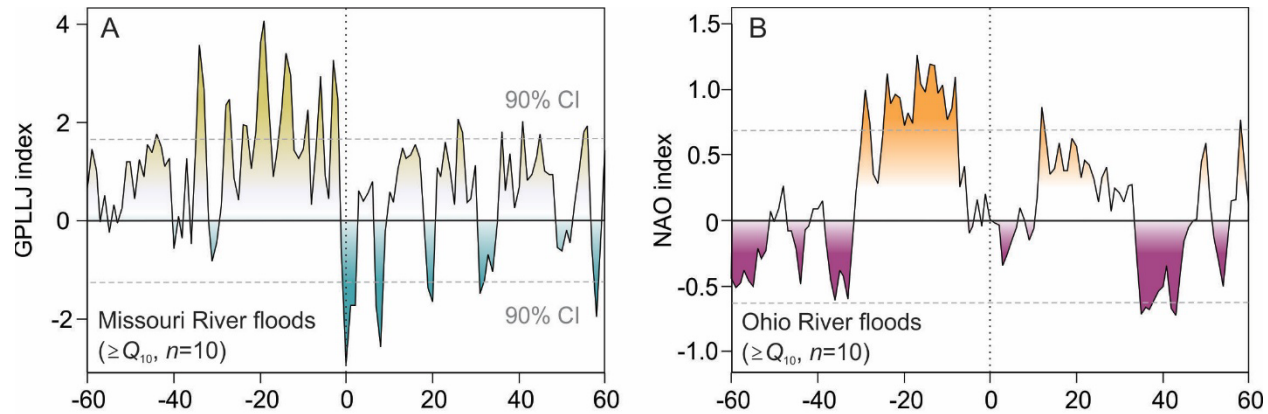


317 **Figure 5.** Evolution of the El Niño-Southern Oscillation (Niño3.4 index) in the 24-months
 318 before and after peak discharge for the ten largest floods on the (A) lower Missouri River and
 319 (B) lower Ohio River.
 320

321 Given the geopotential height and wind anomalies associated with these floods identified in
 322 section 4, we also examined the evolution of GPLLJ and NAO in the weeks preceding and
 323 following the largest floods on the lower Missouri and Ohio Rivers, respectively (Figure 6). For
 324 lower Missouri River floods, the aggregate GPLLJ index consistently exceeds the 90%
 325 confidence interval beginning around 20 days prior to peak discharge through to the flood event
 326

327 itself (Figure 6a). For lower Ohio River floods, the aggregate NAO index of the ten largest
 328 floods exceeds the 90% confidence interval beginning around 25 days prior to peak discharge
 329 and drops below this significance threshold 5 days prior to the flood event (Figure 6b). At an
 330 individual event scale, positive GPLJJ index values occur in the weeks prior to all lower
 331 Missouri River floods (Figure ES4a) and positive NAO values precede all lower Ohio River
 332 floods (Figure ES4b). A positive GPLJJ index, a measure of lower-level (850 hPa) meridional
 333 wind anomalies over the southern Great Plains, reflects the strong and directed southerly winds
 334 off the Gulf of Mexico observed in the month prior to lower Missouri River floods (Figure 2). A
 335 positive NAO, indicating a strong sea level pressure difference between the North Atlantic
 336 Subtropical High and Icelandic Low (Hurrell et al., 2001), is similar to the atmospheric pattern
 337 that triggers lower Ohio River floods (Figure 3) that features an anomalously strong North
 338 Atlantic Subtropical High and promotes advection and convergence of moisture from the Gulf of
 339 Mexico. As atmospheric modes of variability, the GPLJJ and NAO indices exhibit higher
 340 variance than the El Niño-Southern Oscillation and thus offer shorter-term predictive value as a
 341 flood precursor. Our analyses imply that these atmospheric processes work in concert with
 342 oceanic forcing originating in the Pacific to mediate flood occurrence over the major tributaries
 343 of the Mississippi River basin.

344



345 Time to peak discharge (days)
 346 **Figure 6.** Evolution of the (A) Great Plains Low Level Jet (GPLJJ index) and (B) North Atlantic
 347 Oscillation (NAO index) in the 60 days before and after peak discharge for the ten largest floods
 348 on the lower Missouri River and lower Ohio River.
 349

350 We propose that floods on the major tributaries of the Mississippi River system are mediated by
 351 a two-phase process, where antecedent soil moisture mediated by ENSO in the months preceding

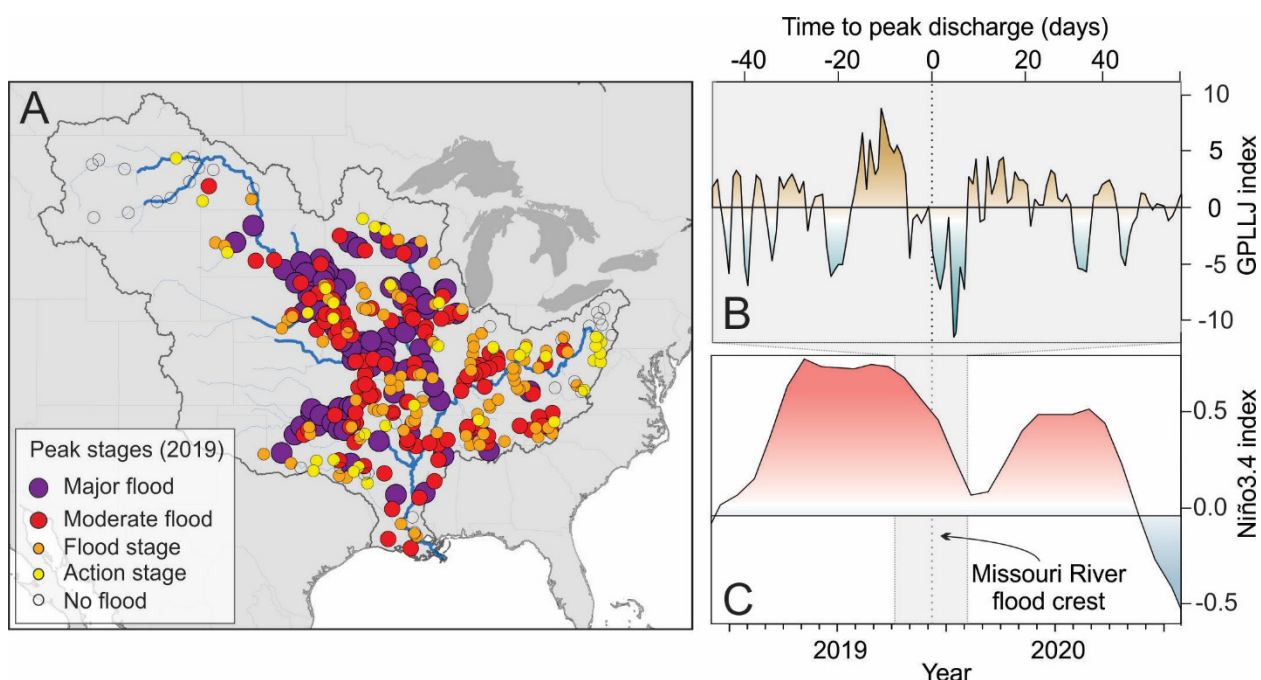
352 an event primes the basin to be vulnerable to flooding, while atmospheric mechanisms (i.e.,
353 GPLJJ and NAO indices) provide the ‘spark’ — an influx of precipitation in the weeks leading
354 up to a flood that generates large amounts of runoff and enhances river discharge. This same
355 ENSO-priming mechanism has previously been identified on the lower Mississippi River
356 (Munoz and Dee, 2017), and here we propose that it extends it to the other major tributaries of
357 the Mississippi River basin. Through its influence on the strength and position of the North
358 Atlantic Subtropical High, the NAO regulates precipitation over the eastern and central parts of
359 the Mississippi River basin, explaining why positive departures of the NAO tend to precede
360 major floods on the lower Ohio River. On the lower Missouri River, where floods tend to occur
361 in the spring and summer months, it is a strong Great Plains Low Level Jet that most often
362 triggers major floods on this tributary. These atmospheric flood triggering mechanisms —
363 namely the strengths of the NAO and GPLJJ — are themselves influenced by modes of ocean-
364 atmosphere variability (Robertson et al. 2000; Walter and Graf 2002; Krishnamurthy et al. 2015).
365 The GPLJJ, in particular, is sensitive to oceanic forcing, with a stronger GPLJJ in boreal
366 spring linked to La Niña while a stronger GPLJJ in boreal summer associated with El Niño
367 (Krishnamurthy et al. 2015), as well as the contrasts in sea surface temperature anomalies
368 between the tropical Pacific and sea surface temperature contrasts and North Atlantic (Malloy
369 and Kirtman 2020).

370

371 **6. 2019 and 2021 floods in hindsight**

372 Major floods occurred within the Mississippi River basin in the water years of 2019 (Figure 7)
373 and 2021 (Figure 8) that illustrate the contrasting mechanisms that generate floods across this
374 basin. In the spring and summer of 2019, major flooding occurred primarily along the Missouri
375 and Mississippi Rivers following an El Niño event that began in the fall of 2018 (Figure 7).
376 During the 2019 water year, 57% of all gages on moderate to large rivers (peak discharge >560
377 m^3/s ; $n=419$) recorded a moderate or major flood stage, with these floods occurring principally
378 along the Missouri, Arkansas, and Mississippi Rivers and their tributaries. These floods began in
379 the spring of 2019, when a series of heavy precipitation events on saturated and/or frozen soils
380 increased river stages along the lower Missouri and Mississippi Rivers (Pal et al., 2020). Positive
381 GPLJJ index values preceded the flood crest on the lower Missouri River by three weeks.

382 Despite flooding over the western and central portions of the Mississippi River basin, flooding
 383 along the lower Ohio River was short-lived and moderate. In contrast to the 2019 floods,
 384 flooding in the winter and spring of 2020/2021 occurred primarily within the Ohio River basin
 385 and was preceded by a La Niña event that began in the fall of 2020 (Figure 8). During the 2021
 386 floods, 21% of all gages on moderate to large rivers recorded a moderate or major flood stage,
 387 with the majority of these floods occurring within the Ohio, lower Mississippi, and Arkansas
 388 sub-basins. Positive NAO index values occurred two weeks prior to the flood crest on the lower
 389 Ohio River.



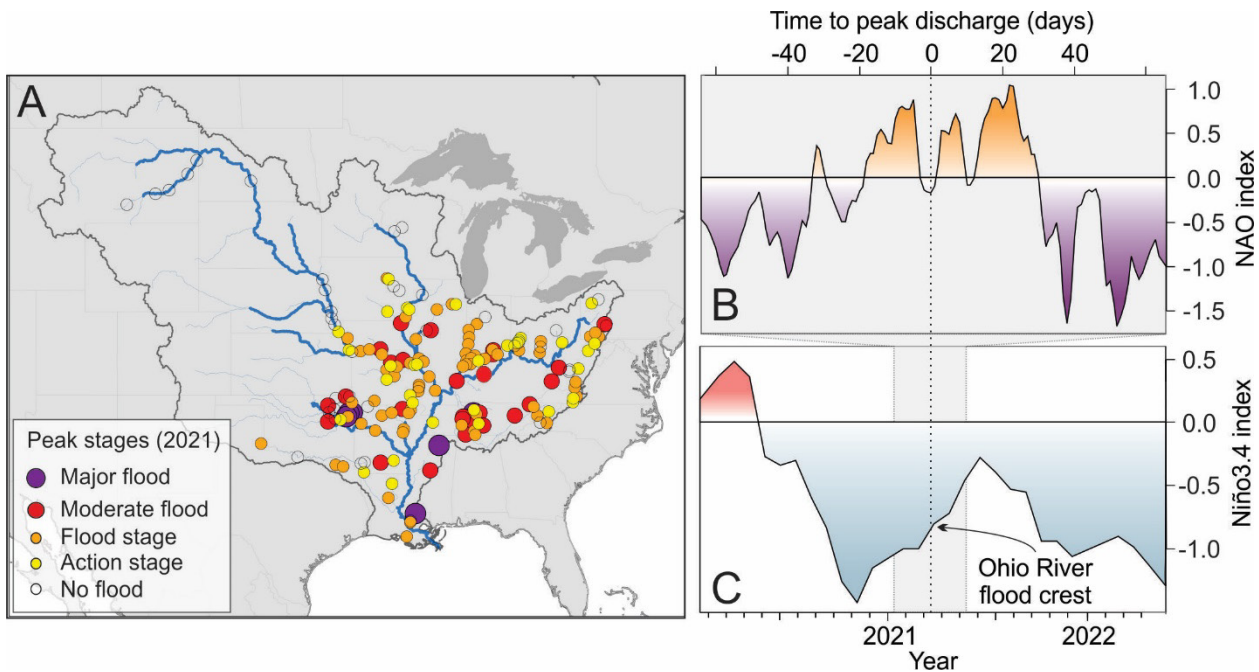
390
 391 **Figure 7.** Hydroclimatic characteristics of the 2019 Missouri-Mississippi River floods: (A) peak
 392 stage categories for the 2019 water year for all moderate to large rivers (peak discharge >560
 393 m^3/s); (B) daily GPLJJ index prior to and following flood crest on the lower Missouri River at
 394 Hermann on June 8 2019; (C) Niño3.4 index (June 2018–June 2020).
 395

396

397

398

399



400

401 **Figure 8.** Hydroclimatic characteristics of the 2021 Ohio River floods: (A) peak stage categories
 402 for the 2021 water year for all moderate to large rivers (peak discharge $>560 \text{ m}^3/\text{s}$); (B) daily
 403 NAO index prior to and following flood crest on the lower Missouri River at Hermann on March
 404 6 2021; (C) Niño3.4 index (March 2020–March 2022).

405

406

407 The pattern of the 2019 and 2021 floods — with major flooding concentrated over the Missouri
 408 and upper Mississippi sub-basins (2019) and Ohio sub-basin (2021) — is consistent with the
 409 oceanic and atmospheric mechanisms that we propose regulate flood hazard within the
 410 Mississippi River basin. Beginning in the fall prior to the floods, ENSO generated positive
 411 precipitation anomalies that saturated soils and served to prime the western (2019) or eastern
 412 (2021) tributary basins to be susceptible to flooding. Then, in the following spring, a series of
 413 heavy precipitation events associated with a positive GPLLJ (2019) and NAO (2021) generated
 414 large amounts of runoff that contributed to major flooding along these tributaries. Spring flood
 415 forecasts issued in late March by the National Weather Service in 2019 and 2021 correctly
 416 identified observed patterns of flooding (NWS 2019; NWS 2021), providing days to weeks of
 417 lead time for the preparation of temporary flood defenses and other mitigation strategies. Our
 418 study implies that the formation of El Niño conditions in the fall of 2018 and La Niña conditions
 419 in the fall of 2020 signaled elevated flood hazard along the lower Missouri River and Ohio
 420 Rivers, respectively — a finding that could have added several months of lead time that could be

421 used to regulate reservoir releases, procure and deploy temporary flood mitigation infrastructure,
422 and develop emergency response plans.

423 **7. CONCLUSIONS**

424 Our results provide a consolidated characterization of the contrasting atmospheric and oceanic
425 mechanisms that generate floods along the principal tributaries of the Mississippi River basin —
426 rivers that form a critical economic corridor for North America. By integrating a climate
427 reanalysis and stream gage records to examine the hydroclimatology of the largest historical
428 floods on the lower Missouri and Ohio Rivers, we identify: (1) the atmospheric mechanisms
429 associated with moisture advection and convergence that trigger high-magnitude floods along
430 these rivers weeks in advance of peak discharge; and (2) the role of the El Niño-Southern
431 Oscillation in mediating antecedent moisture across much of the Mississippi River basin in the
432 months prior to peak discharge. Our findings harbor implications for improving long-range
433 probabilistic flood forecasts, and we note the potential for the interaction of ENSO with other
434 modes of climate variability (Meehl and Teng 2007; Zhou et al. 2014) and variability of ENSO
435 itself (Newman et al. 2011; Luo et al. 2022) to further enhance or suppress flood hazard on these
436 rivers. We also note the potential for land use and river management to exacerbate or ameliorate
437 river stages during a flood independently of climate variability or change (Pinter et al. 2008;
438 Frans et al. 2013). Our work highlights the value of examining commonalities among multiple
439 historical flood events to understand the hydroclimatology of riverine flooding by using publicly
440 available climate reanalysis datasets.

441 **ACKNOWLEDGMENTS**

442 We thank Sylvia Dee, Trevor Porter, Joeri Reinders, Jessica Tierney, and Charlotte Wiman for
443 discussion and comments on this work. This project was supported by grants from the US
444 National Science Foundation (EAR-1804107 and AGS-2147782).

445 **DATA AVAILABILITY STATEMENT**

446 All data used in this study are publicly available: 20th century reanalysis V3
447 (https://psl.noaa.gov/data/gridded/data.20thC_ReanV3.html); Extended Reconstructed Sea
448 Surface Temperature, ERSST v5 (<https://www.ncdc.noaa.gov/data-access/marineocean->

449 [data/extended-reconstructed-sea-surface-temperature-ersst-v5](https://doi.org/10.3133/70000001)); United States Geological Survey
450 (USGS) Water Data for the Nation (<https://waterdata.usgs.gov/nwis>).

451

452 REFERENCES

453 Algarra, I., Eiras-Barca, J., Miguez-Macho, G., Nieto, R., and L. Gimeno, 2019: On the
454 assessment of the moisture transport by the Great Plains low-level jet. *Earth System*
455 *Dynamics*, 10(1), 107-119.

456 Arritt, R. W., Rink, T. D., Segal, M., Todey, D. P., Clark, C. A., Mitchell, M. J., and K.M.
457 Labas, 1997: The Great Plains low-level jet during the warm season of 1993. *Monthly*
458 *weather review*, 125(9), 2176-2192.

459 Camillo, C. A. (2012). *Divine providence: The 2011 flood in the Mississippi River and*
460 *tributaries project*. Mississippi River Commission. US Army Corps of Engineers.
461 Vicksburg, MS.

462 Chen, J., and P. Kumar, 2002: Role of terrestrial hydrologic memory in modulating ENSO
463 impacts in North America. *Journal of Climate*, 15(24), 3569-3585.

464 Coats, S., Smerdon, J. E., Cook, B. I., Seager, R., Cook, E. R., and K.J. Anchukaitis, 2016:
465 Internal ocean-atmosphere variability drives megadroughts in Western North America.
466 *Geophysical Research Letters*, 43(18), 9886-9894.

467 Cook, B. I., Seager, R., and R. L. Miller, 2011: On the causes and dynamics of the early
468 twentieth-century North American pluvial. *Journal of Climate*, 24(19), 5043-5060.

469 Cook, B. I., Smerdon, J. E., Seager, R., and E. R. Cook, 2014: Pan-continental droughts in North
470 America over the last millennium. *Journal of Climate*, 27(1), 383-397.

471 Cook, E. R., Seager, R., Cane, M. A., and D.W. Stahle, 2007: North American drought:
472 Reconstructions, causes, and consequences. *Earth Science Reviews*, 81(1-2), 93-134.

473 Cropper, T., Hanna, E., Valente, M. A., and T. Jónsson, 2015: A daily Azores–Iceland North
474 Atlantic Oscillation index back to 1850. *Geoscience Data Journal*, 2(1), 12-24.

475 Dirmeyer, P. A., and J. L. Kinter III, 2009: The “Maya Express”: Floods in the US Midwest.
476 *Eos, Transactions American Geophysical Union*, 90(12), 101-102.

477 Dirmeyer, P. A., and J. L. Kinter III, 2010: Floods over the US Midwest: A regional water cycle
478 perspective. *Journal of Hydrometeorology*, 11(5), 1172-1181.

479 Enfield, D. B., Mestas-Nuñez, A. M., P. J. Trimble, 2001: The Atlantic multidecadal oscillation
480 and its relation to rainfall and river flows in the continental US. *Geophysical Research
481 Letters*, 28(10), 2077-2080.

482 Frans, C., Istanbulluoglu, E., Mishra, V., Munoz-Arriola, F., and D. P. Lettenmaier, 2013: Are
483 climatic or land cover changes the dominant cause of runoff trends in the Upper
484 Mississippi River Basin?. *Geophysical Research Letters*, 40(6), 1104-1110.

485 Hamlet, A. F., and D. P. Lettenmaier, 1999: Columbia River streamflow forecasting based on
486 ENSO and PDO climate signals. *Journal of Water Resources Planning and Management*,
487 125(6), 333-341.

488 Harding, K. J., and P.K. Snyder, 2015: The relationship between the Pacific–North American
489 teleconnection pattern, the Great Plains low-level jet, and north central US heavy rainfall
490 events. *Journal of Climate*, 28(17), 6729-6742.

491 Helfand, H. M., and S. D. Schubert, 1995: Climatology of the simulated Great Plains low-level
492 jet and its contribution to the continental moisture budget of the United States. *Journal of
493 Climate*, 8(4), 784-806.

494 Higgins, R. W., Yao, Y., Yarosh, E. S., Janowiak, J. E., and K. C. Mo, 1997: Influence of the
495 Great Plains low-level jet on summertime precipitation and moisture transport over the
496 central United States. *Journal of Climate*, 10(3), 481-507.

497 Hirschboeck, K. K., 1988: Flood Hydroclimatology. In *Flood Geomorphology* (ed. by V.R.
498 Baker, R.C. Kochel and P.C. Palton), pp. 27-49. John Wiley & Sons.

499 Hoerling, M., Eischeid, J., and R. Webb, 2013: Understanding and explaining climate extremes
500 in the Missouri River basin associated with the 2011 flooding. *NOAA Climate Assessment
501 Rep*, 34.

502 Huang, B., Thorne, P. W., Banzon, V. F., Boyer, T., Chepurin, G., Lawrimore, J. H., Menne, M.
503 J., Smith, T. M., Vose, R. S., and H. M. Zhang, 2017: Extended reconstructed sea surface
504 temperature, version 5 (ERSSTv5): upgrades, validations, and intercomparisons. *Journal
505 of Climate*, 30(20), 8179-8205.

506 Hurrell, J. W., Kushnir, Y., Ottersen, G., and M. Visbeck, 2003: An overview of the North
507 Atlantic oscillation. *Geophysical Monograph-American Geophysical Union*, 134, 1-36.

508 Hurrell, J. W., Kushnir, Y., and M. Visbeck, 2001: The North Atlantic Oscillation. *Science*,
509 291(5504), 603-605.

510 Feng, S., Hu, Q., and R. J. Oglesby, 2011: Influence of Atlantic sea surface temperatures on
511 persistent drought in North America. *Climate Dynamics*, 37(3-4), 569-586.

512 Keown, M. P., Dardeau Jr, E. A., and E. M. Causey, 1986: Historic trends in the sediment flow
513 regime of the Mississippi River. *Water Resources Research*, 22(11), 1555-1564.

514 Knox, J. C. (2007). The Mississippi River System. *Large Rivers: Geomorphology and*
515 *Management* (ed. by A. Gupta), pp. 145-182, John Wiley & Sons.

516 Krishnamurthy, L., Vecchi, G. A., Msadek, R., Wittenberg, A., Delworth, T. L., and F. Zeng,
517 2015): The seasonality of the Great Plains low-level jet and ENSO relationship. *Journal*
518 *of Climate*, 28(11), 4525-4544.

519 Kunkel, K. E., Changnon, S. A., and J. R. Angel, 1994: Climatic aspects of the 1993 upper
520 Mississippi River basin flood. *Bulletin of the American Meteorological Society*, 75(5),
521 811-822.

522 Li, W., Li, L., Fu, R., Deng, Y., and H. Wang, 2011: Changes to the North Atlantic subtropical
523 high and its role in the intensification of summer rainfall variability in the southeastern
524 United States. *Journal of Climate*, 24(5), 1499-1506.

525 Lincoln, W.S. and D. Graschel, 2016: 2016 Forecast Verifications at the lower Mississippi River
526 Forecast Center using varying QPF. National Weather Service, Technical Report:
527 http://www.weather.gov/media/lmrfc/tech/2016_07_QPF_forecast_verifications.pdf

528 Lincoln, W.S. and D. Graschel, 2018: 2018 Analysis of Gridded Precipitation Estimation
529 Techniques at the Lower Mississippi River Forecast Center. National Weather Service,
530 Technical Report:
531 http://www.weather.gov/media/lmrfc/tech/2018_Analysis_QPE_Techniques.pdf

532 Lo, M. H., and J.S. Famiglietti, 2010: Effect of water table dynamics on land surface hydrologic
533 memory. *Journal of Geophysical Research: Atmospheres*, 115(D22).

534 Lott, G. A. and V. A. Myers, 1956: Meteorology of flood-producing storms in the Mississippi
535 River basin. U.S. Weather Bureau.

536 Luo, X., Dee, S., Stevenson, S., Okumura, Y., Steiger, N., and L. Parsons, 2022: Last
537 Millennium ENSO Diversity and North American Teleconnections: New Insights From
538 Paleoclimate Data Assimilation. *Paleoceanography and Paleoclimatology*, 37(3),
539 e2021PA004283.

540 Mallakpour, I., and G. Villarini, 2016: Investigating the relationship between the frequency of
541 flooding over the central United States and large-scale climate. *Advances in Water
542 Resources*, 92, 159-171.

543 Malloy, K. M., and B.P. Kirtman, 2020: Predictability of midsummer Great Plains low-level jet
544 and associated precipitation. *Weather and Forecasting*, 35(1), 215-235.

545 Meehl, G. A., and H. Teng, 2007: Multi-model changes in El Niño teleconnections over North
546 America in a future warmer climate. *Climate Dynamics*, 29(7), 779-790.

547 Mo, K. C., Paegle, J. N., and R. W. Higgins, 1997: Atmospheric processes associated with
548 summer floods and droughts in the central United States. *Journal of Climate*, 10(12),
549 3028-3046.

550 Muñoz, S. E., and S. G. Dee, 2017: El Niño increases the risk of lower Mississippi River
551 flooding. *Scientific Reports*, 7(1), 1-7.

552 Muñoz, S. E., Giosan, L., Therrell, M. D., Remo, J. W., Shen, Z., Sullivan, R. M., Wiman, C.,
553 O'Donnell, M. and J. P. Donnelly, 2018: Climatic control of Mississippi River flood
554 hazard amplified by river engineering. *Nature*, 556(7699), 95-98.

555 Muñoz, S. E., Porter, T. J., Bakkelund, A., Nusbaumer, J., Dee, S. G., Hamilton, B., Giosan, L.
556 and J. E. Tierney, 2020: Lipid biomarker record documents hydroclimatic variability of
557 the Mississippi River basin during the Common Era. *Geophysical Research Letters*,
558 47(12), e2020GL087237.

559 Nakamura, J., Lall, U., Kushnir, Y., Robertson, A. W., and R. Seager, 2013: Dynamical structure
560 of extreme floods in the US Midwest and the United Kingdom. *Journal of
561 Hydrometeorology*, 14(2), 485-504.

562 National Oceanic and Atmospheric Administration (NOAA, 2016: The National Water Model:
563 Improving NOAA's water prediction service. URL:
564 <https://water.noaa.gov/documents/wrn-national-water-model.pdf>

565 National Weather Service (NWS), 2019: 2019 Spring Flood and Water Resource Outlook. URL:
566 https://www.weather.gov/dvn/2019_springfloodoutlook

567 National Weather Service (NWS), 2021: 2021 Spring Flood and Water Resource Outlook. URL:
568 https://www.weather.gov/dvn/2021_springfloodoutlook

569 Newman, M., Shin, S. I., and M.A. Alexander, 2011: Natural variation in ENSO
570 flavors. *Geophysical Research Letters*, 38(14).

571 NOAA National Centers for Environmental Information (NCEI), 2021: U.S. Billion-Dollar
572 Weather and Climate Disasters. URL: <https://www.ncdc.noaa.gov/billions/>, DOI:
573 10.25921/stkw-7w73

574 Pal, S., Lee, T. R., and N. E. Clark, 2020: The 2019 Mississippi and Missouri River flooding and
575 its impact on atmospheric boundary layer dynamics. *Geophysical Research Letters*,
576 47(6), e2019GL086933.

577 Parrett, C., Melcher, N. B., and R. W. James, 1993: *Flood discharges in the upper Mississippi*
578 *River basin, 1993*. Report No. 1120, US Government Printing Office.

579 Pinter, N., Jemberie, A. A., Remo, J. W., Heine, R. A., and B. S. Ickes, 2008: Flood trends and
580 river engineering on the Mississippi River system. *Geophysical Research Letters*, 35,
581 L23404.

582 Reager, J. T., Thomas, B. F., and J.S. Famiglietti, 2014: River basin flood potential inferred
583 using GRACE gravity observations at several months lead time. *Nature Geoscience*, 7(8),
584 588-592.

585 Robertson, A. W., Mechoso, C. R., and Y. J. Kim, 2000: The influence of Atlantic sea surface
586 temperature anomalies on the North Atlantic Oscillation. *Journal of Climate*, 13(1), 122-
587 138.

588 Ropelewski, C. F., and M. S. Halpert, 1986: North American precipitation and temperature
589 patterns associated with the El Niño/Southern Oscillation (ENSO). *Monthly Weather
590 Review*, 114(12), 2352-2362.

591 Schöngart, J., and W. J. Junk, 2007: Forecasting the flood-pulse in Central Amazonia by ENSO-
592 indices. *Journal of Hydrology*, 335(1-2), 124-132.

593 Seager, R., Kushnir, Y., Herweijer, C., Naik, N., and J. Velez, 2005: Modeling of tropical
594 forcing of persistent droughts and pluvials over western North America: 1856–2000.
595 *Journal of Climate*, 18(19), 4065-4088.

596 Slivinski, L. C., Compo, G. P., Whitaker, J. S., Sardeshmukh, P. D., Giese, B. S., McColl, C.,
597 Allan, R., Yin, X., Vose, R., Titchner, H., Kennedy, J., Spencer, L. J., Ashcroft, L.,
598 Brönnimann, S., Brunet, M., Camuffo, D., Cornes, R., Cram, T. A., Crouthamel, R.,
599 Domínguez-Castro, F., Freeman, J. E., Gergis, J., Hawkins, E., Jones, P. D., Jourdain, S.,
600 Kaplan, A., Kubota, H., Le Blancq, F., Lee, T., Lorrey, A., Luterbacher, J., Maugeri, M.,
601 Mock, C. J., Moore, G. K., Przybylak, R., Pudmenzky, C., Reason, C., Slonosky, V. C.,
602 Smith, C., Tinz, B., Trewin, B., Valente, M. A., Wang, X. L., Wilkinson, C., Wood, K.
603 and Wyszyński, P., 2019: Towards a more reliable historical reanalysis: Improvements
604 for version 3 of the Twentieth Century Reanalysis system. *Quarterly Journal of the Royal
605 Meteorological Society*, 145(724), 2876-2908.

606 Smith, J. A., and M. L. Baeck, 2015: “Prophetic vision, vivid imagination”: The 1927
607 Mississippi River flood. *Water Resources Research*, 51(12), 9964-9994.

608 Smith, L. M., and B. R. Winkley, 1996: The response of the Lower Mississippi River to river
609 engineering. *Engineering Geology*, 45(1-4), 433-455.

610 Smith, J. A., Baeck, M. L., Ntelekos, A. A., Villarini, G., and M. Steiner, 2011: Extreme rainfall
611 and flooding from orographic thunderstorms in the central Appalachians. *Water
612 Resources Research*, 47(4).

613 Therrell, M. D., and M. B. Bialecki, 2015: A multi-century tree-ring record of spring flooding on
614 the Mississippi River. *Journal of Hydrology*, 529, 490-498.

615 Thomson, A. M., Brown, R. A., Rosenberg, N. J., Izaurrealde, R. C., Legler, D. M., and R.
616 Srinivasan, 2003: Simulated impacts of El Niño/Southern Oscillation on United States

617 water resources. *JAWRA Journal of the American Water Resources Association*, 39(1),
618 137-148.

619 Trenberth, K. E., 1997: The definition of El Niño. *Bulletin of the American Meteorological
620 Society*, 78(12), 2771-2778.

621 United States Geological Survey (USGS), 2021: USGS Water Data for USA. URL:
622 <https://waterdata.usgs.gov/nwis?>

623 Walter, K., and H.F. Graf, 2002: On the changing nature of the regional connection between the
624 North Atlantic Oscillation and sea surface temperature. *Journal of Geophysical
625 Research: Atmospheres*, 107(D17), ACL-7.

626 Wang, S. Y., and T. C. Chen, 2009: The late-spring maximum of rainfall over the US central
627 plains and the role of the low-level jet. *Journal of Climate*, 22(17), 4696-4709.

628 Wang, G., and E. A. Eltahir, 1999: Use of ENSO information in medium-and long-range
629 forecasting of the Nile floods. *Journal of Climate*, 12(6), 1726-1737.

630 Weaver, S. J., and S. Nigam, 2008: Variability of the Great Plains low-level jet: Large-scale
631 circulation context and hydroclimate impacts. *Journal of Climate*, 21(7), 1532-1551.

632 Wise, E. K., Woodhouse, C. A., McCabe, G. J., Pederson, G. T., and J. M. St-Jacques, 2018:
633 Hydroclimatology of the Missouri River basin. *Journal of Hydrometeorology*, 19(1), 161-
634 182.

635 Zhang, W., and G. Villarini, 2019: On the weather types that shape the precipitation patterns
636 across the US Midwest. *Climate Dynamics*, 53(7), 4217-4232.

637 Zhou, Z. Q., Xie, S. P., Zheng, X. T., Liu, Q., and H. Wang, 2014: Global warming-induced
638 changes in El Niño teleconnections over the North Pacific and North America. *Journal of
639 Climate*, 27(24), 9050-9064.